

Image-Based Marker-Free Screening of GABA_A Agonists, Antagonists, and Modulators

SLAS Discovery
2020, Vol. 25(5) 458–470
© 2019 The Author(s)



DOI: 10.1177/2472555219887142
journals.sagepub.com/home/jbx



Benjamin Rappaz¹, Pascal Jourdain^{2,3}, Damiano Banfi¹, Fabien Kuttler¹,
Pierre Marquet^{2,3,4}, and Gerardo Turcatti¹ 

Abstract

The ionotropic GABA_A receptors represent the main target for different groups of widely used drugs having hypnotic and anxiolytic effects. So far, most approaches used to assess GABA activity involve invasive low-throughput electrophysiological techniques or rely on fluorescent dyes, preventing the ability to conduct noninvasive and thus nonperturbing screens. To address this limitation, we have developed an automated marker-free cell imaging method, based on digital holographic microscopy (DHM). This technology allows the automatic screening of compounds in multiple plates without having to label the cells or use special plates.

This methodological approach was first validated by screening the GABA_A receptor expressed in HEK cells using a selection of active compounds in agonist, antagonist, and modulator modes. Then, in a second blind screen of a library of 3041 compounds (mostly composed of natural products), 5 compounds having a specific agonist action on the GABA_A receptor were identified. The hits validated from this unbiased screen were the natural products muscimol, neurosteroid alphaxalone, and three compounds belonging to the avermectin family, all known for having an agonistic effect on the GABA_A receptor. The results obtained were exempt from false negatives (structurally similar unassigned hits), and false-positive hits were detected and discarded without the need for performing electrophysiological measurements.

The outcome of the screen demonstrates the applicability of our screening by imaging method for the discovery of new chemical structures, particularly regarding chemicals interacting with the ionotropic GABA_A receptor and more generally with any ligand-gated ion channels and transporters.

Keywords

quantitative phase imaging, digital holographic microscopy, GABA_A, high-content screening, ligand-gated ion channels

Introduction

Chloride homeostasis has a pivotal role in controlling neuronal excitability in the adult brain as well as during neurodevelopment. The intracellular concentration of chloride is regulated by the dynamic equilibrium between passive fluxes resulting from the operations of both plasma membrane chloride channels and local impermeant anions as well as the active fluxes mediated by transporters. Chloride channels are involved in several physiological functions such as cell volume regulation, transmembrane fluid transport, muscular activity, and neuroexcitability (for review see Duran et al.¹). Their dysfunction is observed in more than a dozen human pathological conditions, including several that affect the nervous system, such as epilepsy and certain psychiatric diseases (for review see Bowery and Smart²). The development of drugs targeted to these chloride ion channels represents an important field for developing novel pharmaceutical agents and the need for anxiolytics

and hypnotics with fewer side effects than the benzodiazepines (for review Kowalczyk and Kulig³). Specifically, a complete understanding of the physiological GABAergic

¹Biomolecular Screening Facility (BSF), Ecole Polytechnique Fédérale de Lausanne (EPFL), Lausanne, Switzerland

²Joint International Research Unit in Child Psychiatry, Département de Psychiatrie CHUV, University of Lausanne, Switzerland

³Université Laval, Québec, QC, Canada

⁴Centre de Recherche CERVO, Québec, QC, Canada

Received July 24, 2019, and in revised form Sept 20, 2019. Accepted for publication Oct 16, 2019.

Supplemental material is available online with this article.

Corresponding Author:

Gerardo Turcatti, Biomolecular Screening Facility (BSF), Ecole Polytechnique Fédérale de Lausanne (EPFL), Station 15, Lausanne, 1015, Switzerland.

Email: gerardo.turcatti@epfl.ch

activity requires a full quantification of the dynamic properties of GABA-activated chloride channels.

In general, electrophysiology (patch clamp) remains the most accurate technique for analyzing and quantifying the effectiveness of a drug on ligand-gated ion channels. Thus, this approach has been widely used for studying chloride currents mediated by GABA_A. Nevertheless, despite an exceptional fidelity and precision, patch clamp is a priori not suitable for multiple compound screening since this approach is technically demanding, with very low-throughput capacity, labor-intensive, and limited to single-cell assay.

However, the recent development of automated patch clamp systems⁴ has substantially improved the throughput (e.g., Patchliner and SyncroPatch 384/768PE [Nanion Technologies GmbH, Munich, Germany]; CytoPatch [Cytocentrics AG, Rostock, Germany]; PatchXpress 7000A, IonWorks Quattro, and IonWorks Barracuda [Molecular Devices, LLC, San Jose, CA, USA]; Dynaflo Resolve [flucell, Gothenburg, Sweden]; QPatch and Qube [Sophion A/S, Ballerup, Denmark]; IonFlux Mercury HT [Fluxion Bioscience Inc., Alameda, CA, USA]), yet with the requirement to have cells in suspension before the experiments, thus limiting potential maturation of the monitored cells and precluding experiments on primary culture. The invasive aspect of cytoplasm dilution by the content of the pipette is also often neglected. Besides the important contribution of automated patch clamp systems to drug discovery, the unpredictable gigaohm seal and the absence of visual inspection have still limited the screening of large random compound sets.

A widely used approach to monitor the dynamics of intracellular chloride is the use of fluorescent dyes whose signal is related to the intracellular concentration of chloride (for review see Arosio and Ratto⁵). However, despite the advantage of a wide range of fluorophores allowing for the measurement of multiple targets and high-throughput capabilities,⁶ the technique suffers from several methodological drawbacks, including low sensitivity and specificity, limitations inherent to the loading and washing steps of the protocol, pH sensitivity of the dye, and photobleaching and phototoxicity. In addition, the quantitative determination of intracellular chloride concentration changes with nonelectrophysiological methods amenable to screening approaches has been challenging, in particular because the transmembrane ratio of chloride is low (10:1) and the equilibrium potential of chloride is generally close to the resting membrane potential of cells. These two factors result in minute chloride concentration changes, therefore raising issues of sensitivity.⁵ Time-lapse experiments using living cells with fluorescent dyes are challenging to implement routinely and imply high running cost due to the price of fluorescent dyes. Furthermore, the image focusing process required prior to image acquisition itself is time-consuming.⁷ These disadvantages consequently yield a reduced throughput and a cost

per data point that may represent an issue for some screening settings.

The fluorescence lifetime of fluorescence molecules has also been successfully used to accurately measure intracellular chloride concentration changes,⁶ while requiring expensive dedicated apparatus. All genetically encoded chloride sensors are also responding to other changes in their surroundings, like pH,⁸ which might be a problem knowing that GABA_A receptors are also permeable to bicarbonate, which modulates the pH, therefore affecting imaging as well.⁵

Due to the above drawbacks, several approaches relying on label-free screening methods have been implemented in drug discovery for a variety of assays, enabling noninvasive and sensitive measurements of many cellular responses, including receptor activation, signaling, ion channel activation, cell growth and proliferation, cell differentiation, and cell migration.⁹ These label-free-based biosensors convert the cell stimulus into a cell-induced quantifiable signal through an optical or electrical transducer. For example, the commercial instruments Epic BT (Corning) and BIND (SRU Biosystems) make use of resonance waveguide gratings to generate an evanescent wave to sense whole-cell responses.¹⁰ Other instruments, for example, ECIS (Applied BioPhysics), xCELLigence (Acea Biosciences), and CellKey (Molecular Devices), rely on a low electrolyte impedance interface to detect the impedance of a cell layer under sinusoidal-voltage-generated electric fields.¹¹ All in all, these label-free technologies are still currently not optimal for their application in image-based screening assays, due to their lack of satisfactory spatial resolution for studies at the single-cell level and their high associated consumable costs.¹²

In addition to the above-mentioned microscopy techniques, quantitative phase imaging (QPI) represents a group of label-free microscopy techniques (reviewed in Park et al.¹³) that enable the provision of quantitative phase images of transparent living cells, allowing visualization of cell structures and dynamics. The QPI we have developed, called quantitative phase digital holographic microscopy (QP-DHM), presents the great advantage, thanks in particular to a numerical autofocus capability,¹⁴ to accurately measure, under extended periods of time (up to a few days), the optical path difference (OPD) (see eq 1). From these accurate OPD measurements, various biophysical parameters have been derived, including absolute cell volume, dry mass, and protein concentration.¹⁵ Furthermore, QP-DHM represents an efficient tool to perform both early detection of cell death^{12,16} and monitoring of ligand-gated ion channel activity. The osmotic-driven water flux accompanying ionic movements related to the channel activity can indeed be monitored by DHM, as it significantly changes the intracellular refractive index (see eq 1).^{15,17,18}

The suitability of QP-DHM for image-based screening in multiwell cell culture plates¹² and for time-lapse measurement has recently been confirmed. In the present paper, we first validated, in 96-well plates, the capability of QP-DHM to perform agonist/antagonist and modulator screens using a targeted selection of compounds on HEK cells expressing the α_1 , β_2 , and γ_2 s subunits of the GABA_A ion-channel receptors. Second, in 384-well plates, we performed a blind agonist screen on a collection of natural products and compounds synthesized in Swiss chemistry groups. All hits were then further characterized with QP-DHM and confirmed with electrophysiology.

Materials and Methods

Library Design

First, a specific “GABA compounds” library was created for our validation assays. We selected all the entries of the 1280 FDA-approved compounds of Prestwick Chemical Library (PCL; Illkirch, France) that had the keyword “GABA” in their annotations (20 compounds). We then added 11 compounds from other suppliers known to have effects on GABA receptors (based on a literature search). Those 31 compounds were then used as seeds to identify other compounds having structural similarities in the 14,000 compounds of the Maybridge HitFinder (MHF) library (Maybridge, UK) and the PCL. Compounds were considered similar to one of the seeds if they exhibited a Tanimoto distance¹⁹ of less than 0.4 when using an extended connectivity fingerprint of diameter 4. This allowed the selection of 13 and 9 additional compounds, respectively. A description of all 53 selected compounds, their therapeutic group, and mechanism of action can be found in **Supplemental Table S1**. All compounds were dissolved at 10 mM in 100% DMSO and used at 10 μ M (0.1% DMSO), a DMSO concentration that has no measurable effect on the readout (see **Suppl. Fig. S1**).

A second blind screen library was composed of 3041 compounds: 2627 from a “Natural products” library with compounds obtained from Analyticon (Germany) and InterBioscreen (Russia) that are purified organic molecules from fractionated extracts of two sources, plants and bacteria. The 414 remaining compounds are diverse and synthesized and kindly provided by various academic laboratories in Switzerland through the ACCESS platform (The Swiss Chemical Collection; <https://nccr-chembio.ch/technologies/facilities/the-swiss-chemical-collection/>).

Cell Culture

HEK 293 cells stably expressing the α_1 , β_2 , and γ_2 s subunits of the rat GABA_A receptors (HEK-GABA) were generously given by Hoffmann-La Roche (Basel, Switzerland). Details

on the constructs can be found in a previous publication.¹⁷ After thawing, cells were grown in minimal essential medium (Invitrogen) supplemented with 10% fetal calf serum (Invitrogen) and 20 mM HEPES (Invitrogen) for 2 days, and then the cells were transferred to the same medium, also containing the following selection antibiotics: 0.3 μ g/mL puromycin (Clontech, Mountain View, CA), 300 μ g/mL hygromycin B (Roche Diagnostics, Mannheim, Germany), and 200 μ g/mL G418 (Invitrogen).

For all experiments, medium was replaced by an artificial cerebrospinal fluid (ACSF) containing (in mM) NaSCN, 140; KCl, 3; D-glucose, 5; HEPES, 10; CaCl₂, 3; and MgCl₂, 2 (pH 7.4; 290–295 mOsm; room temperature). Usually, the extracellular medium contains NaCl instead of NaSCN. However, in the NaCl condition, the reversal potential for chloride (E_{Cl}) is the same as the membrane potential, causing a net Cl⁻ flux close to zero even if the GABA_A receptor is open. NaCl substitution by NaSCN allows changing the equilibrium for chloride at the membrane resting potential of the GABA_A receptor,¹⁷ a prerequisite for measuring GABA activity.

For QP-DHM imaging, HEK-GABA cells were plated on 0.1 mg/mL poly-L-ornithine (Sigma, catalog number P3655)-coated 96-well imaging plates (Falcon, catalog number 353219) or 384-well imaging plates (Falcon, catalog number 353962), at 40,000 cells (96-WP) or 10,000 cells (384-WP) per well, and used at 4 days in vitro (DIV) with a change of culture medium at 3 DIV. With 384-well plates, we observed a nonnegligible border effect (due to evaporation); thus, the two external rows on each border were not used. At 4 DIV, the culture medium is replaced with ACSF containing the compounds to test. As NaSCN induces a small drift of the QP-DHM-measured signals,¹⁷ one row of the medium is replaced every 30 s (corresponding to the scanning time for one row) using a robotic liquid handling dispenser and two columns are used as references to subtract the small drift in the recorded signal due to NaSCN.¹⁷

For electrophysiological recordings, cells were grown on a 20 mm glass coverslip coated with 0.1 mg/mL poly-L-ornithine used at 4 DIV with a change of culture medium at 3 DIV and placed on a recording chamber perfused using a peristaltic pump with ACSF containing the compounds to test.

Electrophysiology Recording

For all experiments, HEK_{GABA} cells were transferred to an open recording chamber and perfused in an ACSF containing (in mM) NaCl, 140; KCl, 3; D-glucose, 5; HEPES, 10; CaCl₂, 3; and MgCl₂, 2 (pH 7.4; 290–295 mOsm; room temperature). HEK_{GABA} cells were voltage clamped at a holding potential of -40 mV.

Whole-cell recordings were made at room temperature, and signals were amplified using a Multiclamp 700B amplifier (Axon Instruments, Union City, CA) and digitized by

means of an ITC-1600 interface (Instrutech, Great Neck, NY) to a PC computer running Igor Pro (Wavemetrics, Portland, OR). All currents (sampling interval, 5 kHz) were low-pass-filtered (2 kHz). They were recorded with pipettes containing (in mM) potassium-gluconate, 95; KCl, 40 (equal to intracellular HEK cell concentration²⁰); HEPES, 10; and MgCl₂, 2 (pH 7.3; 280–290 mOsm). Gluconate is an impermeant anion used place of proteins to prevent dilution of the intracellular content. The pipettes were pulled with a DMZ universal puller.

GABA and all compounds were dissolved in ACSF and applied by bath perfusion during 30 s at concentrations ranging from 1 nM to 100 μM. A delay of at least 10 min was observed between successive applications.

The effect of each compound concentration was obtained by measuring the maximum current for each recorded current curve (see Fig. 3 and Suppl. Fig. S2).

DHM Image Acquisition

For each experiment, four images per well were acquired and the corresponding measurements were averaged to yield a mean value per well. DHM quantitative images were acquired at room temperature (~22 °C) on a commercially available DHM T-1001 from LynceeTec SA (Lausanne, Switzerland) equipped with a motorized *xy* stage (Märzhäuser Wetzlar GmbH & Co. KG, Wetzlar, Germany, catalog number S429). Images were recorded using a Leica 10×/0.22 NA objective (Leica Microsystems GmbH, Wetzlar, Germany, catalog number 11506263). The typical acquisition time is less than 0.5 ms per image and the total scan time (with four images per well) is 3 min 40 s for 96-well plates, and 8 min for 384-well plates (when the two outer wells are not imaged), both resulting in a single-row scan time of about 30 s. Images are automatically numerically refocused to the best focus after the acquisition.¹²

Label-Free QP-DHM Technology

Briefly, QP-DHM^{21–23} is a label-free interferometric microscopy technique that provides a quantitative measurement of the optical path length (OPL; related to the optical density of the cell). It is a two-step process where a hologram consisting of a 2D interference pattern is first recorded on a digital camera and the contrast (phase) images are reconstructed numerically using a specific algorithm.²⁴ The contrast in the QP-DHM phase images is quantitatively related to the OPD, expressed in terms of physical properties as

$$OPD(x, y) = d(x, y) \cdot [n_m - \bar{n}_c(x, y)], \quad (1)$$

where $d(x, y)$ is the cell thickness, $\bar{n}_c(x, y)$ is the mean *z*-integrated intracellular refractive index at the (x, y) position,

and n_m is the refractive index of the surrounding culture medium. Simply put, eq 1 means that the OPD signal is proportional to both the cell thickness and the intracellular refractive index, a property linked to the protein and water content of the cells.¹⁵ QP-DHM systems generally use a low-intensity laser as a light source for specimen illumination and a digital camera to record the hologram. Here, the 684 nm laser source delivers 200 μW/cm² at the specimen plane—that is some six orders of magnitude less than intensities typically associated with confocal fluorescence microscopy. With that amount of light, the exposure time is only 400 μs.

As described in Jourdain et al.,¹⁷ when Cl[−] is replaced by SCN[−] in bath solution, the Cl[−] gradient is reversed with a Cl[−] intracellular concentration (around 40 mM in HEK cells; see Gillen and Forbush²⁰) higher than the extracellular one (13 mM). Thus, activation of the GABA_A receptor by a specific ligand will produce an efflux of Cl[−], together with an exit of molecules of water (for osmotic reasons), leading to both a cell shrinkage and an increase of the intracellular refractive index.¹⁷ As OPD is highly sensitive to intracellular refractive index changes,¹⁵ the net signal will be a significant OPD increase (Fig. 1).

Data Analysis

Confluency was measured by first thresholding the images with a fixed predetermined value to obtain a mask and then by measuring the surface ratio of the mask to the total area of the field of view. The total OPD value is obtained by adding the OPD value recorded in each of the (x, y) masked pixels of the image. Finally, the average OPD is obtained by dividing the total OPD by the surface of the mask and is a measure of the optical density of the cells within the field of view independently of the confluency. This value is dependent on the cell shape (rounded cells have a higher optical density than flat cells). The average OPD is an unbiased parameter that can be used to categorize cell phenotypes¹² or quantify the activity of ion channels.^{17,18}

Dose-response curves were fitted using Prism7 (GraphPad Software, La Jolla, CA) with the following equation:

$$Y = Bottom + \frac{Top - Bottom}{1 + 10^{-(\log EC_{50} - X) * Hillslope}}, \quad (2)$$

where X is the log concentration of compounds, Y is the measured average OPD response, Top and $Bottom$ are the plateaus of the average OPD response, $Hillslope$ is the slope factor or Hill slope, and $\log EC_{50}$ is the fitted logarithm of the half-maximal effective concentration. For the QP-DHM and electrophysiology agonist EC₅₀ ranking experiments, the Hill slope was set at 2 (which corresponds

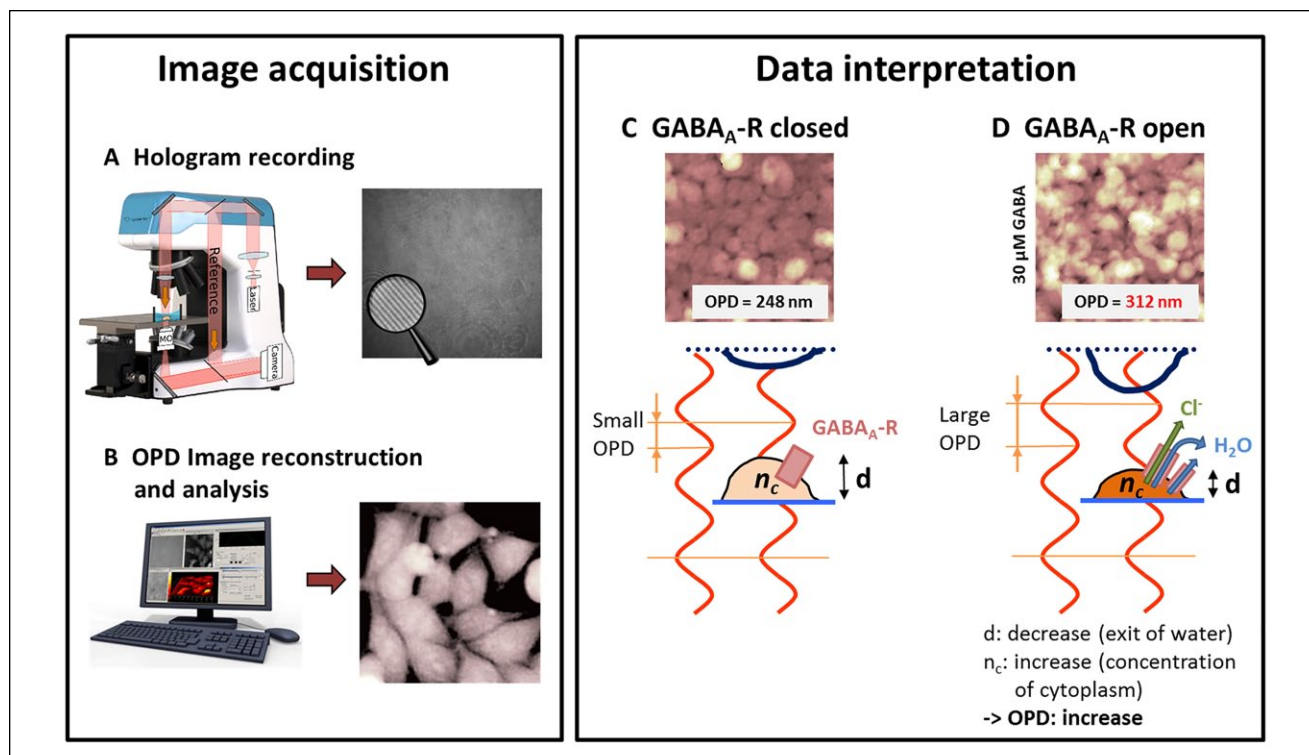


Figure 1. DHM workflow and OPD signal interpretation when HEK-GABA cells are stimulated by GABA. Image acquisition: Holograms are (A) acquired with the DHM setup and (B) reconstructed numerically to generate quantitative phase images. Image analysis is then performed. (C) Cells in the resting condition. (D) Data interpretation: When the GABA_A receptor is activated, ion and water exit the cells, leading to an intracellular refractive index raise that increases the average OPD, which is the final readout used to monitor the activity of the GABA_A receptor.

to the two binding sites of GABA) for all the fittings. For the antagonist experiments, the Hill slope was not fixed, and for the modulator experiments the Hill slope was not fitted (fixed at 1).

All data are represented as means \pm standard error of the mean (SEM).

Three separated types of screen were conducted in duplicate using the GABA library: agonist, antagonist, and modulator.

Before running the screens, the GABAEC₃₀ (EC₃₀ GABA) and EC₇₀ (EC₇₀ GABA) values were measured in four separate experiments where a serial dilution (3 points per log) of GABA was applied for 8 min; values were calculated using the following equation:

$$EC_{F\text{GABA}} = \left(\frac{F}{100 - F} \right)^{1/H} \cdot EC_{50}, \quad (3)$$

where F is the fraction (in percent, 30 or 70 in our case) and H is the fitted Hill slope.

The agonist screen aims to identify direct agonists of the GABA_A receptor where compounds are added directly to

the cells. The antagonist screen aims to identify direct antagonists of the GABA_A receptor. Compounds are added together with GABA at its EC₇₀ concentration (EC₇₀ GABA) and the inhibition of the response is measured. The modulator screen aims to identify modulators of the GABA_A receptor. Compounds are added together with GABA at its EC₃₀ concentration (EC₃₀ GABA) and the potentiation of the response is measured. The second blind screen was done in an agonist search mode.

Data from the screens were imported in a custom-made laboratory information management system (LIMS). To compare the relative effect of each compound, raw values were first normalized for each plate against the corresponding controls, bringing the negative control value to 0 and the positive control value to 1. Hits were defined as values 3 standard deviations (SD) above the negative controls (0 μM GABA), 3 SD above the measured EC₃₀ GABA value (0.4 μM GABA), or 3 SD below the measured EC₇₀ GABA value (1.2 μM GABA) for the agonist and blind screens, modulator, and antagonist screens, respectively. Normalized values of the hits were then averaged between duplicates to produce a final score for the screened compounds.

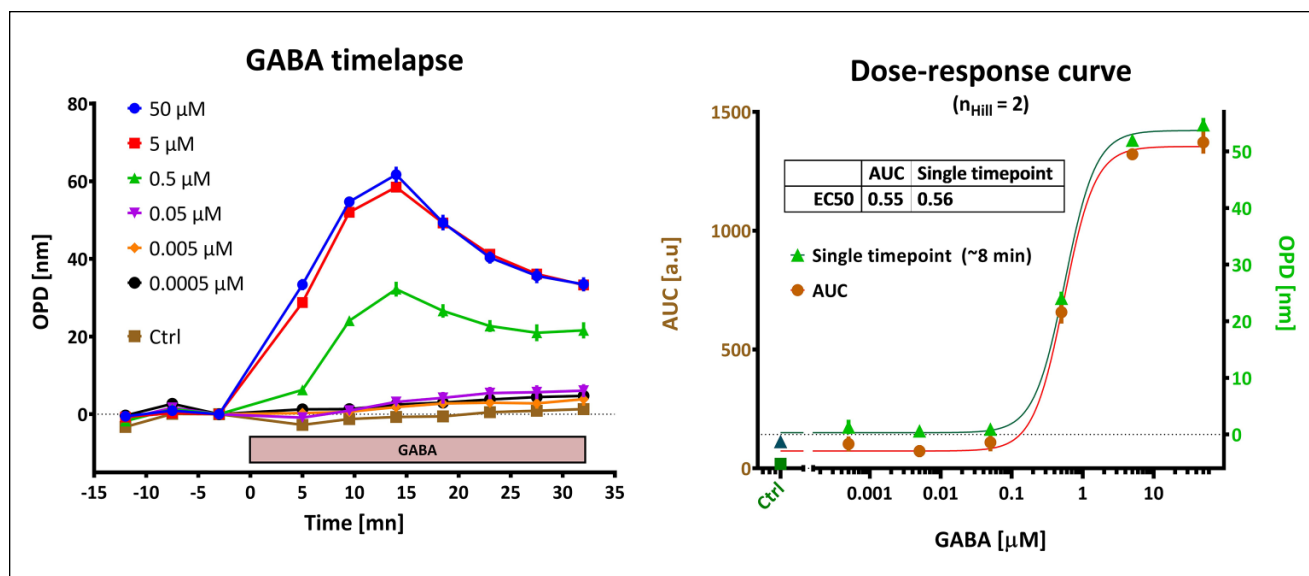


Figure 2. Assay development. Left: Dynamics of the GABA signal recorded in a 96-well plate. We observe a prolonged effect with a peak at 8–14 min after the start of stimulation. Right: Quantification. The whole dynamics was integrated by measuring the area under the curve (AUC) and compared with a single time-point measurement (at 8 min); both approaches yield the same EC₅₀ value.

Results

Assay Development

The QP-DHM technique has been previously validated for GABA activity monitoring¹⁷ using a peristaltic pump to deliver a pulse of GABA on single coverslips containing HEK-GABA cells. However, to adapt the technique to high-throughput screening or high-content screening, modifications must be conducted to accommodate imaging using microtiter plates. With our current system, culture medium is replaced by the assay medium containing GABA and/or other compounds using a robotic liquid handling dispenser. When four images are acquired by well, the whole 96-well plate can be imaged in less than 4 min. Time-lapse acquisition of serial dilution of GABA (Fig. 2) allowed us to optimize the timing for image acquisition (between 8 and 12 min after medium replacement). Afterward, we observed a decline of the signal even though GABA is still present in the well, corresponding to the GABA receptor desensitization²⁵ and to a reduction of the chloride gradient due to the efflux of the ion. The longer time (minutes vs seconds) required to obtain a maximal response compared with electrophysiology is due to the signal integration aspect of QP-DHM,¹⁷ which is sensitive to the number of ions having passed through the membrane. Consistently, we accessed the EC₅₀ of GABA by simply measuring the effect at a single time point (8 min) after medium replacement, which is also the timing we used for all the screening assays.

Plating density and culture duration were optimized to yield the best assay conditions, quantified by the Z' factor,²⁶

a direct measure of the quality of an assay, where a value close to 1 indicates an excellent screening window, whereas a value below 0.5 reflects a marginal assay. Our culture conditions (see Materials and Methods) yielded reproducible Z' factors in the 0.6–0.8 range for 96-WP and around 0.5–0.7 for 384-WP.

Validation Screens

Hits obtained for the agonist, antagonist, and modulator screens are given in **Supplemental Table S2** together with their normalized score. We found eight hits for the agonist screen, nine hits for the modulator screen, and five hits for the antagonist screen. We excluded from further analysis the modulator hits that were also agonist hits at the assay conditions.

The eight compounds that were hits for the agonist screen were retested in serial dilution using QP-DHM imaging and validated with electrophysiological recording (Fig. 3A,B and Suppl. Fig. S2).

All compounds were confirmed as hits and results from the QP-DHM agonist screen were in good agreement with the results obtained with electrophysiology (Fig. 3B and Suppl. Table S3) except for ivermectin and avermectin B1a, which have a ~10× higher EC₅₀ value with electrophysiology, suggesting a lower affinity when measured with this method. This discrepancy can be explained by both the rise time, which is about 500 times longer (for ivermectin) than that for GABA, and the absence of desensitization (for both).²⁷ Since with QP-DHM the compounds

are not washed, they have more time to produce an effect (especially with both a low rise-time and a lack of desensitization), resulting in a lower estimated EC_{50} value. Avermectin B1a has a dose-dependent effect (activation or inhibition),²⁸ shortened rise time, and persistent effect,²⁹ leading to a larger total ion flux when the compounds are not washed, and thus can similarly explain the higher EC_{50} value recorded by electrophysiology in our conditions. Nevertheless, QP-DHM is in very good agreement with the reported EC_{50} value of 1.9 μM .²⁹

The five compounds that were hits for the antagonist screen were retested in serial dilution (Fig. 3C).

The antagonist hits were confirmed, and all produced a nearly complete inhibition of the effect of GABA at its EC_{70} concentration (1.2 μM ; Fig. 3C). The reported IC_{50} values for bicuculline were 0.53 μM in the presence of 10 μM GABA³⁰ and 0.9 μM in the presence of 3 μM GABA;³¹ for thiocolchicoside, 0.15 to 0.9 μM according to neuron type;³² for gabazine, ~0.2 μM in the presence of 3 μM GABA;³¹ and for picrotoxin, 3.1 μM in the presence of 10 μM GABA,³⁰ all in very good agreement with the QP-DHM results.

From the nine modulator hits, only two showed a score higher than 0.5 (zaleplon and colchicine); those were also the only two that we confirmed (i.e., that could be fitted with a sigmoid curve) when retested in serial dilutions. The maximum concentration of zaleplon and colchicine increased the effect of GABA to 41% or 21% of the maximum (GABA at 10 μM), respectively (Fig. 3D).

Zaleplon has also previously been reported as a modulator with an EC_{50} of 0.17 μM with $\alpha 1\beta 2\gamma 2$ expressed in *Xenopus* oocytes.³³ However, the obtained effect of colchicine is in apparent disagreement with what has been reported in the literature, for which colchicine significantly inhibits GABA currents recorded from L(tk⁻) cells stably transfected with human $\alpha 1\beta 2\gamma 2\text{L}$ GABA_A receptor subunits.³⁴ Colchicine was included based on its structure homology with thiocolchicoside, which exhibited an antagonist effect in the EC_{70} antago-screen, an effect also described in the literature: thiocolchicoside-inhibited GABA-evoked Cl^- currents with similar potencies (median inhibitory concentrations of 0.2 μM for $\alpha 1\beta 2\gamma 2\text{L}$ receptors) and in a competitive manner were reported.³⁵ Colchicine inhibits GABA_A receptors independently of microtubule depolymerization.³⁶

This discrepancy could be explained by a dual effect of colchicine, increasing the OPD on one side by acting on the cytoskeleton, and having an antagonist effect on the other side.³⁷ This is confirmed by the fact that a significant delay in OPD increase is observed when colchicine is applied for more than 15 min, demonstrating that the effect of this compound on microtubule dynamics has a retarded influence on OPD signal increase compared with its effect on GABA signal transduction. We thus concluded that the observed effect

of colchicine is mainly due to an increased OPD signal induced by microtubule depolymerization. This highlights the need to carefully design experimental conditions and controls to specifically observe the monitored process.

Blind Screen

On the 3041 compounds tested for agonist effect, 15 hits (defined as 3 SD above the negative controls) were obtained, corresponding to a hit rate of 0.49% (Suppl. Table S4).

Each compound, as well as GABA, was further retested, in serial dilution (nine dilutions from 100 μM to 0.01 μM in triplicate). To validate the specificity of the GABA response, each compound was added at its calculated EC_{70} value (concentration that produces 70% of the maximal response, estimated using the GraphPad Prism Find EC_{anything} function) alone or with either 100 μM picrotoxin (a noncompetitive channel blocker for GABA_A receptor) or 100 μM bicuculline (a competitive antagonist of GABA_A receptor). Compounds that have a very steep Hill slope were also tested at 3 \times their EC_{70} value. All tests were performed using both wild-type HEK cells (HEK-WT³⁸) and HEK cells expressing the GABA-R used in this study ($\alpha 1$, $\beta 2$, and $\gamma 2\text{s}$ subunits, HEK-GABA). Wild-type HEK cells show no electrophysiological response to GABA when tested with patch clamp¹⁷ and thus serve as an additional control for the specificity of the response. Tests done on HEK-WT used standard culture medium, whereas tests with HEK-GABA used artificial ACSF medium.

Among the 15 original hits, 6 were found to be active and specific for the GABA_A receptor (muscimol, avermectin B1A, 17 α -hydroxypregnanolone, alphaxalone, emamectin B1A, and eprinomectin B1A), 7 were found to be nonspecific (indicated by the beige rectangle in Fig. 4), and 2 were found to have a marginal effect (vindesine and colchicine), even when retested at 3 \times their estimated EC_{70} concentration. Dose-response curves of the validated hits can be found in Supplemental Figure 3.

Table 1 describes the six retained specific and validated hits from the primary screen. Muscimol, which was present in the collection screened, was detected as an agonist delivering pharmacological parameters as reported and was also obtained in our pilot screen in the agonist mode. Besides this well-known agonist detected without prior knowledge of the content of the chemical collection, the other compounds belong to two distinct chemical families (neurosteroid and avermectin-like) based on their structure. Alphaxalone is a neurosteroid previously reported as a potentiator and agonist at high concentration.³⁹ The compound STOCK1N-56888 detected in the primary screening has been discarded due to quality control issues. This compound, which was annotated by the supplier to be 17 α -hydroxypregnanolone, did not pass our quality control check by liquid chromatography-mass spectrometry

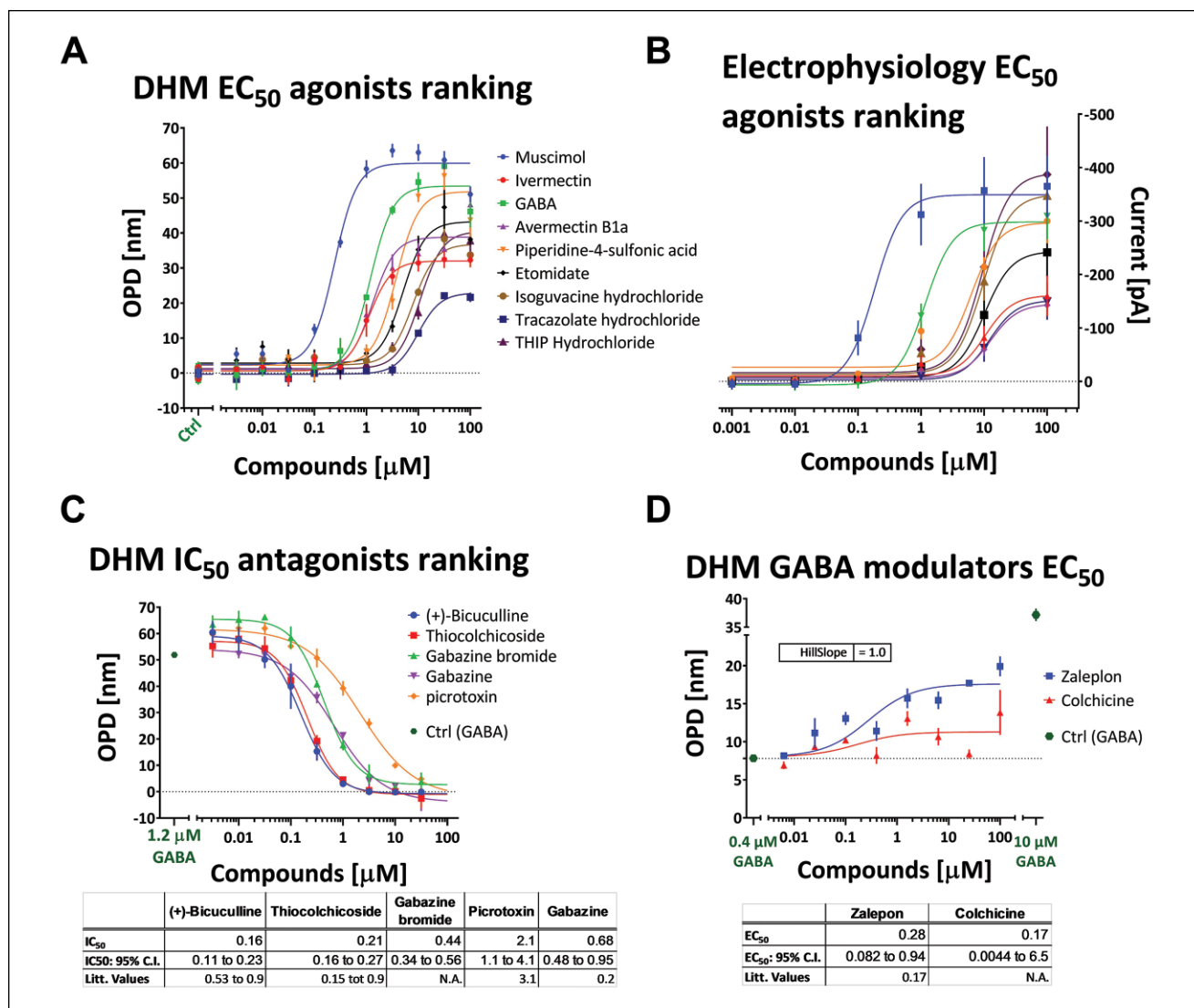


Figure 3. Hits analysis and validation. **(A,B)** Agonist hit validation and EC₅₀ ranking. Hits from the agonist screen were retested in serial dilution and measured with DHM **(A)** and electrophysiology **(B)**. The Hill slope was fixed at 2 for all compounds to ease the comparison between the two modalities. Complete data are provided in Supplemental Table S3. Typical current recordings at different GABA concentrations are shown in Supplemental Figure S2. **(C)** Antagonist hit validation and IC₅₀ ranking. Gabazine and gabazine bromide are identical with the exception of a bromide anion (Br⁻). The compounds were tested together with GABA at its EC₇₀ value (1.2 µM). The table provides the measured IC₅₀ values together with their 95% confidence interval (C.I.) ranges and the values reported in the literature (references in the main text). N.A. = not available. **(D)** Modulators of the GABA receptor with their respective EC₅₀ values. The compounds were tested together with GABA at its EC₃₀ value (0.4 µM). The table provides the measured EC₅₀ values together with their 95% confidence interval ranges and the values reported in the literature (references in the main text). N.A. = not available. Values obtained at 10 µM can be compared with the results of the primary screen shown in Supplemental Table 4.

(LC-MS) for peak purity and mass assignment (data not shown). Since the mass obtained for this compound was the same as that for alphaxalone, the two compounds were co-injected and analyzed by LC. Two distinct well-resolved peaks were obtained demonstrating that the compound STOCK1N-56888 cannot be alphaxalone. Further NMR analyses confirmed that the supplied compound was not the expected one. However, even if a neurosteroid backbone is

suggested by our data, an unambiguous structural assignment was not possible; therefore, this compound was not retained as a validated hit. Moreover, the structure corresponding to 17 α -hydroxypregnanolone is not following the structure–activity relationship (SAR) rules for GABA_A active neurosteroids,⁴⁰ suggesting that the compound delivered as 17 α -hydroxypregnanolone could be another active neurosteroid or a mixture (Suppl. Fig. S4). This mistake

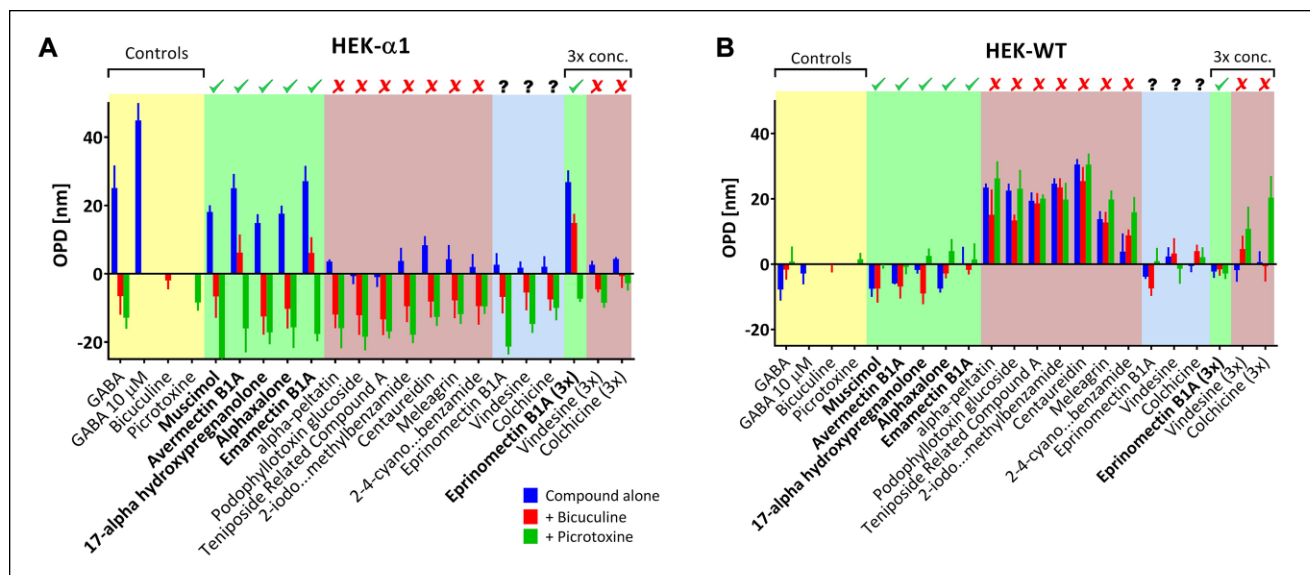


Figure 4. Hits validation. **(A)** Inhibition test: Each compound was tested alone or with either picrotoxin or bicuculine on HEK cells expressing the GABA_A receptor. Only compounds that had an effect inhibited by the two drugs were considered specific for GABA_A receptors. **(B)** Specificity test: Compounds were tested on wild-type HEK cells not expressing the GABA_A receptor. Compounds producing an effect are nonspecific for the GABA_A receptor (indicated by the beige rectangles in both graphs). Three compounds had a low effect at the calculated EC₇₀ value (blue rectangle) and were thus retested at 3× this concentration. Hits that were validated by these two tests are in bold.

Table I. List of Preliminary Validated Hits.

Validated Hits	EC ₅₀ (μM)	Hill Coefficient	Amplitude (%)	Name	Purity (%)	Expected Mass Observed by ESI (Positive Mode)
Muscimol	0.2	1.9	100	Muscimol	>95	Yes
STOCK IN-51728	1.5–1.7	1.6–1.8	60	Alphaxalone	>95	Yes
STOCK IN-56888	1.3–1.6	2.1–2.3	54	17α-hydroxypregnanolone	90	No; the same mass as alphaxalone was obtained
STOCK IN-67743	6.9	6.3	94	Avermectin B1a	75	Yes
STOCK IN-65883	5.6	5.4	87	Emamectin B1a	73	Yes
STOCK IN-63866	5.5	5.4	79	Eprinomectin B1a	45	Yes

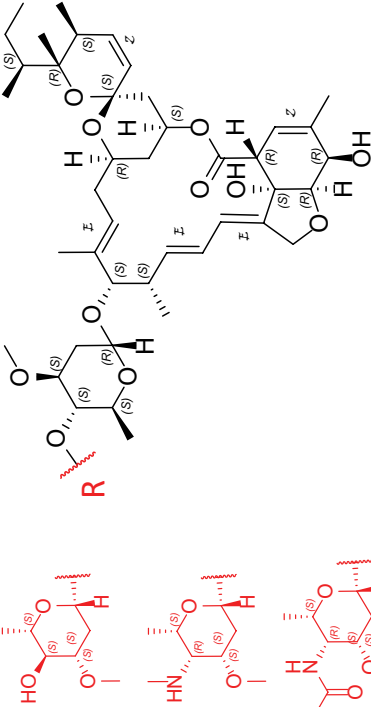
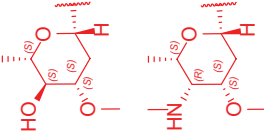
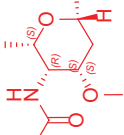
The data obtained from the dose–response curves of validated hits are reported as well as the purity determined by LC. The last column reports the correlation of the expected mass and the observed one analyzed by electrospray (ESI)–MS (in positive mode). The compound STOCK IN-56888 did not pass the quality control test and analytical data obtained do not correspond to the structure provided by the supplier.

from the chemical compound supplier that we were able to detect highlights the need for thorough quality control of compounds used in chemical screening and in particular for validating hits.

The natural products collection used for the screen was in silico screened for structures bearing steroids following

the SAR rules for GABA_A activity. No other molecules were detected, confirming that our screen was free from false negatives regarding the neurosteroid compounds. One molecule present in our collection and negative in our assay was alphaxalone acetylated at the 3α OH on the A steroid ring. This is consistent with the neurosteroid SAR rules,⁴⁰

Table 2. Structures and Pharmacological Data of GABA_A Active Compounds from the Natural Products Screen Belonging to the Avermectin Family.

Catalog ID	Name	CAS Registry No.	EC ₅₀ (μM)	Hill Coefficient	Amplitude (%)	R
STOCKIN-67743	Avermectin B1a	65195-55-3	6.9	6.3	94	
STOCKIN-65883	Emamectin B1a	121124-29-6	5.6	5.4	87	
STOCKIN-63866	Eprinomectin B1a	133305-88-1	5.5	5.4	79	

where a hydrogen bond-donating group is necessary for triggering GABA_A activity.

The structures of the three other compounds belonging to the family of avermectins are illustrated in **Table 2**. Avermectins are antiparasitic agents, 16-membered macrocyclic lactones with a disaccharide substituent at the carbon-13 position. Avermectin B1a has been reported as a partial agonist at the high-affinity state and also binding other sites of the GABA_A receptor.²⁸ Avermectin B1a, emamectin B1a, and eprinomectin B1a, possessing a high structural similarity, delivered very similar parameters from the dose–response curves, namely, EC₅₀ and Hill coefficients. Our measured Hill coefficient of 5–6 suggests multiple molecules binding per pentameric receptor, in agreement with a recent report suggesting that ivermectin, also a member of the avermectin family, binds to the GABA_A receptor in a common orientation at each of the five interfaces.⁴¹

It is important to emphasize that no other avermectin-like structures were present in the collection of natural products screened (no false negatives), confirming and validating that our screen by the QP-DHM imaging method is robust and accurate for the assignment of GABA_A-activating molecules.

Discussion

In this paper we presented a GABA_A receptor screen using a marker-free motorized QP-DHM. The activity of the receptor is quantified thanks to the ion-associated water fluxes' impact on the refractive index. The specificity of the signal is validated by the inhibition of the measured effect by antagonists and the absence of effect of the reported compounds in wild-type cells not expressing the GABA_A receptor. Furthermore, we also confirmed that QP-DHM was not limited to the system model tested in this report by also ranking the potency of five known agonists using HEK cells expressing the $\alpha 5\beta 3\gamma 2$ receptor subtype and comparing the results with electrophysiological recordings (**Suppl. Fig. S5**).

QP-DHM is intrinsically multisite in its recording, as each of the pixels in the image provide a quantitative measurement of the activity of the monitored receptors. A high sensitivity can therefore be obtained by averaging the measurements over all the cells present in the field of view, as demonstrated in this paper, or individual cells can be measured and tracked over time-lapse acquisitions in parallel recordings^{12,18,42} or used to distinguish different phenotypes.⁴³ Like with fluorescent-based high-content screening images, QP-DHM images could even be used in repurposing assays, to go deeper into the analysis of alternative pathways or targets.⁴⁴ QP-DHM images also offer a direct visual quality control of the experiments (visualizing the images allows the eventual discrimination of wells with contamination, growth problems, or any other issues that might affect the measurement). In contrast to QP-DHM, other label-free

techniques should rely on additional quality control steps to assess the integrity of the cell culture.

Compared with electrophysiology, which measures net currents through the membrane related to the fluxes of ions, the phase signal recorded by QP-DHM is proportional to the temporal integration of these ion fluxes.¹⁷ The dynamics measured with the two approaches is thus different, in the second timescale for electrophysiology and in the minute timescale for QP-DHM. Some small differences observed between the two techniques, notably when receptor desensitization occurred (like with ivermectin), can also be explained by the fact that compounds were only applied for 30 s and then washed out with electrophysiology (bath application in open perfusion chamber) or applied continuously (inside well plate without perfusion) for QP-DHM. However, this less rapid timescale offers a larger time frame for imaging and provides more versatility for recording the cell response. In addition, the overall time needed to perform the experiments was much smaller. For instance, the data presented in **Figure 3A** were obtained and analyzed automatically in a 1 h experiment with QP-DHM (from the scan of a 96-well plate in duplicate), while 3 days of multiple-cell patching for electrophysiology from an experienced user was required (**Fig. 3B**).

The method presented here has been validated first with a set of selected compounds and compared with electrophysiological measurements. The results obtained from the larger blind screen constituted an additional confirmation of the robustness and applicability of the approach in a high-throughput context where identified specific GABA_A agonists were validated without the need for further electrophysiology-based experiments. The false-positive compounds (compounds that were hits in the screen but later discarded as also being active in the validation test on wild-type HEK cells) were α -peltatin, podophyllotoxin glucoside, teniposide-related compound A, centaureidin, meleagrins, vindesine, and colchicine, as well as two compounds from the Swiss Chemical Collection, provided by the same academic lab, and both derivatives of benzamide backbones. Among these nine compounds, seven are known to target directly or indirectly the dynamics of microtubules, mainly through inhibition of tubulin polymerization (the other two being original molecules not previously described). It is therefore expected that such compounds, acting on microtubule dynamics, can ultimately display an effect on almost all cellular processes besides the potential GABAergic effect, whatever the readout, but mainly linked to differences in timings, reflecting differences in modes of action. For instance, meleagrins is a precursor of oxalins (similar to roquefortine) and classified as a tremorgenic mycotoxin, which is thought to inhibit the GABA receptor and have an effect on microtubules.⁴⁵

In summary, the results reported in this publication demonstrate that the activity of the GABA_A receptor can be

successfully monitored and new chemical structures specifically interfering with this activity can be discovered using the label-free image-based DHM system. We propose this new approach for primary screening and preliminary validation of hits. It can then be followed by low-throughput complete characterization using standard electrophysiological techniques.

This drug discovery tool can be extended to other ion-channel targets of therapeutic interest, like the glutamate receptor,¹⁸ the CFTR receptor,⁴² or even electroneutral cotransporters (like NKCC1 and KCC2),¹⁸ which cannot be assessed by electrophysiology due to the net neutral charge being transported, but still can be analyzed by DHM through monitoring of the net flux of water.

Acknowledgments

The authors thank the BSF team for their technical assistance, in particular Nathalie Ballanfat, Jonathan Vesin, Julien Bortoli Chapalay, and Antoine Gibelin.

Declaration of Conflicting Interests

The authors disclosed receipt of the following potential conflicts of interest with respect to the research, authorship, and/or publication of this article: B.R. also works part-time for Lyncee Tec, which commercializes the DHM used in this study. The other authors declare no conflicts of interest. The work presented in this study was performed independently of B.R.'s work at Lyncee Tec.

Funding

The authors disclosed receipt of the following financial support for the research, authorship, and/or publication of this article: Part of this work was supported by the CTI program (grant no. 12669.1 PFLS-LS). We acknowledge the national research program NCCR Chemical Biology and the Swiss National Science Foundation for their financial support. We also acknowledge the support of the University of Lausanne and Departement de Psychiatrie-CHUV to the International Joint Research Unit in Child Psychiatry.

ORCID iD

Gerardo Turcatti  <https://orcid.org/0000-0003-0139-223X>

References

- Duran, C.; Thompson, C. H.; Xiao, Q.; et al. Chloride Channels: Often Enigmatic, Rarely Predictable. *Annu. Rev. Physiol.* **2010**, *72*, 95–121.
- Bowery, N. G.; Smart, T. G. GABA and Glycine as Neurotransmitters: A Brief History. *Br. J. Pharmacol.* **2006**, *147* (Suppl. 1), S109–S119.
- Kowalczyk, P.; Kulig, K. GABA System as a Target for New Drugs. *Curr. Med. Chem.* **2014**, *21*, 3294–3309.
- Milligan, C. J.; Moller, C. Automated Planar Patch-Clamp. *Methods Mol. Biol.* **2013**, *998*, 171–187.
- Arosio, D.; Ratto, G. M. Twenty Years of Fluorescence Imaging of Intracellular Chloride. *Front. Cell. Neurosci.* **2014**, *8*, 258.
- Gagnon, M.; Bergeron, M. J.; Lavertu, G.; et al. Chloride Extrusion Enhancers as Novel Therapeutics for Neurological Diseases. *Nat. Med.* **2013**, *19*, 1524–1528.
- Neumann, B.; Held, M.; Liebel, U.; et al. High-Throughput RNAi Screening by Time-Lapse Imaging of Live Human Cells. *Nat. Methods* **2006**, *3*, 385–390.
- Jose, M.; Nair, D. K.; Reissner, C.; et al. Photophysics of Clomeleon by FLIM: Discriminating Excited State Reactions along Neuronal Development. *Biophys. J.* **2007**, *92*, 2237–2254.
- Fang, Y. Label-Free Biosensors for Cell Biology. *Int. J. Electrochem.* **2011**, *2011*, 460850.
- Fang, Y.; Ferrie, A. M.; Fontaine, N. H.; et al. Resonant Waveguide Grating Biosensor for Living Cell Sensing. *Biophys. J.* **2006**, *91*, 1925–1940.
- McGuinness, R. Impedance-Based Cellular Assay Technologies: Recent Advances, Future Promise. *Curr. Opin. Pharmacol.* **2007**, *7*, 535–540.
- Kuhn, J.; Shaffer, E.; Mena, J.; et al. Label-Free Cytotoxicity Screening Assay by Digital Holographic Microscopy. *Assay Drug Dev. Technol.* **2013**, *11*, 101–107.
- Park, Y.; Depeursinge, C.; Popescu, G. Quantitative Phase Imaging in Biomedicine. *Nat. Photonics* **2018**, *12*, 578–589.
- Fatih Toy, M.; Kuhn, J.; Richard, S.; et al. Accelerated Autofocusing of Off-Axis Holograms Using Critical Sampling. *Opt. Lett.* **2012**, *37*, 5094–5096.
- Rappaz, B.; Marquet, P.; Cuche, E.; et al. Measurement of the Integral Refractive Index and Dynamic Cell Morphometry of Living Cells with Digital Holographic Microscopy. *Opt. Express* **2005**, *13*, 9361–9373.
- Pavillon, N.; Kühn, J.; Moratal, C.; et al. Early Cell Death Detection with Digital Holographic Microscopy. *PLoS One* **2012**, *7*, e30912.
- Jourdain, P.; Boss, D.; Rappaz, B.; et al. Simultaneous Optical Recording in Multiple Cells by Digital Holographic Microscopy of Chloride Current Associated to Activation of the Ligand-Gated Chloride Channel GABA(A) Receptor. *PLoS One* **2012**, *7*, e51041.
- Jourdain, P.; Pavillon, N.; Moratal, C.; et al. Determination of Transmembrane Water Fluxes in Neurons Elicited by Glutamate Ionotropic Receptors and by the Cotransporters KCC2 and NKCC1: A Digital Holographic Microscopy Study. *J. Neurosci.* **2011**, *31*, 11846–11854.
- Tanimoto, T. T. *An Elementary Mathematical Theory of Classification and Prediction by T.T. Tanimoto*; International Business Machines Corporation: New York, 1958.
- Gillen, C. M.; Forbush, B., III. Functional Interaction of the K-Cl Cotransporter (KCC1) with the Na-K-Cl Cotransporter in HEK-293 Cells. *Am. J. Physiol.* **1999**, *276*, C328–C336.
- Anand, A.; Chhaniwal, V. K.; Javidi, B. Imaging Embryonic Stem Cell Dynamics Using Quantitative 3-D Digital Holographic Microscopy. *IEEE Photonics J.* **2011**, *3*, 546–554.
- Carl, D.; Kemper, B.; Wernicke, G.; et al. Parameter-Optimized Digital Holographic Microscope for High-Resolution Living-Cell Analysis. *Appl. Opt.* **2004**, *43*, 6536–6544.
- Curl, C. L.; Bellair, C. J.; Harris, P. J.; et al. Quantitative Phase Microscopy: A New Tool for Investigating the Structure and

- Function of Unstained Live Cells. *Clin. Exp. Pharmacol. Physiol.* **2004**, *31*, 896–901.
24. Marquet, P.; Rappaz, B.; Magistretti, P. J.; et al. Digital Holographic Microscopy: A Noninvasive Contrast Imaging Technique Allowing Quantitative Visualization of Living Cells with Subwavelength Axial Accuracy. *Opt. Lett.* **2005**, *30*, 468–470.
 25. Chang, Y.; Ghansah, E.; Chen, Y.; et al. Desensitization Mechanism of GABA Receptors Revealed by Single Oocyte Binding and Receptor Function. *J. Neurosci.* **2002**, *22*, 7982–7990.
 26. Zhang, J.-H.; Chung, T. D. Y.; Oldenburg, K. R. A Simple Statistical Parameter for Use in Evaluation and Validation of High Throughput Screening Assays. *J. Biomol. Screen.* **1999**, *4*, 67–73.
 27. Adelsberger, H.; Lepier, A.; Dudel, J. Activation of Rat Recombinant Alpha(1)Beta(2)Gamma(2S) GABA(A) Receptor by the Insecticide Ivermectin. *Eur. J. Pharmacol.* **2000**, *394*, 163–170.
 28. Huang, J.; Casida, J. E. Avermectin B1a Binds to High- and Low-Affinity Sites with Dual Effects on the Gamma-Aminobutyric Acid-Gated Chloride Channel of Cultured Cerebellar Granule Neurons. *J. Pharmacol. Exp. Ther.* **1997**, *281*, 261–266.
 29. Schonrock, B.; Bormann, J. Activation of Cl⁻ Channels by Avermectin in Rat Cultured Hippocampal Neurons. *Naunyn Schmiedebergs Arch. Pharmacol.* **1993**, *348*, 628–632.
 30. Tang, W.; Wildey, M. J. Development of a Colorimetric Method for Functional Chloride Channel Assay. *J. Biomol. Screen.* **2004**, *9*, 607–613.
 31. Ueno, S.; Bracamontes, J.; Zorumski, C.; et al. Bicuculline and Gabazine Are Allosteric Inhibitors of Channel Opening of the GABAA Receptor. *J. Neurosci.* **1997**, *17*, 625–634.
 32. Carta, M.; Murru, L.; Botta, P.; et al. The Muscle Relaxant Thiocolchicoside Is an Antagonist of GABAA Receptor Function in the Central Nervous System. *Neuropharmacology* **2006**, *51*, 805–815.
 33. Sanna, E.; Busonero, F.; Talani, G.; et al. Comparison of the Effects of Zaleplon, Zolpidem, and Triazolam at Various GABA(A) Receptor Subtypes. *Eur. J. Pharmacol.* **2002**, *451*, 103–110.
 34. Weiner, J. L.; Buhler, A. V.; Whatley, V. J.; et al. Colchicine Is a Competitive Antagonist at Human Recombinant Gamma-Aminobutyric Acid A Receptors. *J. Pharmacol. Exp. Ther.* **1998**, *284*, 95–102.
 35. Mascia, M. P.; Bachis, E.; Obili, N.; et al. Thiocolchicoside Inhibits the Activity of Various Subtypes of Recombinant GABA(A) Receptors Expressed in *Xenopus laevis* Oocytes. *Eur. J. Pharmacol.* **2007**, *558*, 37–42.
 36. Bueno, O. F.; Leidenheimer, N. J. Colchicine Inhibits GABA(A) Receptors Independently of Microtubule Depolymerization. *Neuropharmacology* **1998**, *37*, 383–390.
 37. Rappaz, B.; Kuttler, F.; Breton, B.; et al. Digital Holographic Imaging for Label-Free Phenotypic Profiling, Cytotoxicity, and Chloride Channels Target Screening. In *Label-Free Biosensor Methods in Drug Discovery*; Fang, Y., Ed.; Springer: New York, 2015; pp 307–325.
 38. Hamilton, B. J.; Lennon, D. J.; Im, H. K.; et al. Stable Expression of Cloned Rat GABAA Receptor Subunits in a Human Kidney Cell Line. *Neurosci. Lett.* **1993**, *153*, 206–209.
 39. Cottrell, G. A.; Lambert, J. J.; Peters, J. A. Modulation of GABAA Receptor Activity by Alphaalone. *Br. J. Pharmacol.* **1987**, *90*, 491–500.
 40. Reddy, D. S. Neurosteroids: Endogenous Role in the Human Brain and Therapeutic Potentials. *Progress Brain Res.* **2010**, *186*, 113–137.
 41. Estrada-Mondragon, A.; Lynch, J. W. Functional Characterization of Ivermectin Binding Sites in $\alpha 1\beta 2\gamma 2L$ GABA(A) Receptors. *Front. Mol. Neurosci.* **2015**, *8*, 55.
 42. Jourdain, P.; Becq, F.; Lengacher, S.; et al. The Human CFTR Protein Expressed in CHO Cells Activates Aquaporin-3 in a cAMP-Dependent Pathway: Study by Digital Holographic Microscopy. *J. Cell. Sci.* **2014**, *127*, 546–556.
 43. Rappaz, B.; Breton, B.; Shaffer, E.; et al. Digital Holographic Microscopy: A Quantitative Label-Free Microscopy Technique for Phenotypic Screening. *Comb. Chem. High Throughput Screen.* **2014**, *17*, 80–88.
 44. Simm, J.; Klambauer, G.; Arany, A.; et al. Repurposing High-Throughput Image Assays Enables Biological Activity Prediction for Drug Discovery. *Cell Chem. Biol.* **2018**, *25*, 611–618.e3.
 45. Koizumi, Y.; Arai, M.; Tomoda, H.; et al. Oxaline, a Fungal Alkaloid, Arrests the Cell Cycle in M Phase by Inhibition of Tubulin Polymerization. *Biochim. Biophys. Acta Mol. Cell Res.* **2004**, *1693*, 47–55.